Volume 13
Number 33
7 September 2025
Pages 10061–10374

Journal of Materials Chemistry B

Materials for biology and medicine

rsc.li/materials-b

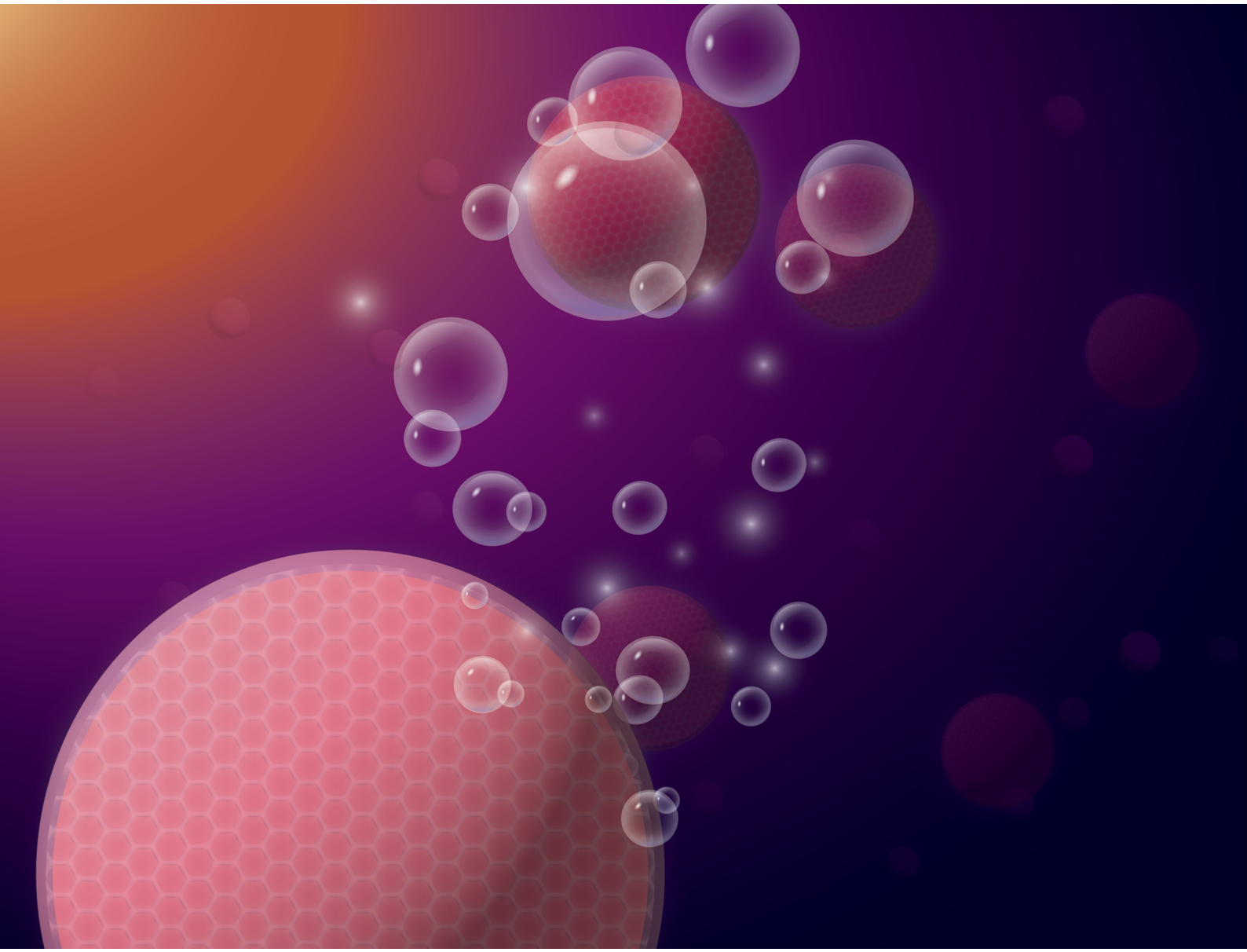

ISSN 2050-750X

ROYAL SOCIETY OF CHEMISTRY

PAPER
Ariel L. Furst *et al.*
Self-assembled nanomaterials enable extended lithium release

Journal of Materials Chemistry B

ROYAL SOCIETY OF CHEMISTRY

PAPER

View Article Online
View Journal | View Issue

Check for updates

Cite this: J. Mater. Chem. B, 2025, 13, 10170

Self-assembled nanomaterials enable extended lithium release†

Marjon Zamani,[a] Kirmina Monir[a] and Ariel L. Furst *[ab]

Received 17th April 2025,
Accepted 14th July 2025

DOI: 10.1039/d5tb00901d

rsc.li/materials-b

Lithium is the gold-standard treatment for bipolar disorder, which impacts over 5.7 million US adults. Yet, this treatment has a narrow therapeutic range that is dangerously close to toxic levels. Though extended-release lithium formulations exist, they necessitate frequent serum monitoring and cause adverse effects in nearly one in ten patients. Here, we report a novel lithium formulation with improved release kinetics. By coating alginate microparticles with lithium-doped metal phenolic networks (MPNs), lithium release is maintained within a safe, therapeutically relevant range for an unprecedented 100 hours. Release studies show lithium concentrations reaching their peak in serum after 11 hours, more than twice as long as existing formulations, with maintenance of therapeutic levels for at least four days. This novel lithium formulation is the first to offer such tight control over lithium concentration in serum for such an extended time, providing the potential to revolutionize lithium therapy and vastly improve patient experience with this medication.

Introduction

Bipolar disorder (BD) impacts nearly 2.5% of the global population[1] and nearly six million adults in the US.[2] BD is characterized by major depression, euthymia, and mania, leading to severe impairment in over 80% of those diagnosed[3] and an economic burden of $195 billion each year in the US alone.[3] Despite the diversity in BD presentation, there has been only one gold-standard BD treatment for over 70 years: lithium therapy. Lithium (Li^+) is prescribed for both acute and long-term BD and is the only treatment proven to prevent both the manic and depressive episodes that are characteristic of this disorder.[4] Yet, lithium remains challenging and burdensome for patients to adhere to due to its extremely narrow therapeutic range (0.6–1.2 mM serum concentration). Further, toxicity occurs at 1.5 mM, making precise dosing imperative.[5] Ensuring sufficient lithium in serum without reaching toxic levels requires frequent blood draws (usually weekly) until dosing is stabilized.[6] This regimen is restrictive and negatively impacts patient quality of life and compliance.

Though dosing is a known challenge with lithium, its formulation has remained essentially unchanged since its introduction. Current products consist of either citrate or carbonate lithium salts in immediate release (IR) or prolonged release (PR) formulations.[7] IR products reach peak plasma concentrations one to two hours after administration and can be given up to three times per day. PR formulations reach their peak concentrations between four and five hours after administration and are usually taken once daily. Though PR formulations have fewer adverse effects than IR (9.1% compared to 18.3%)[7] and are more popular with patients, they still cause a lithium spike following administration and necessitate frequent serum monitoring. To improve the safety, efficacy, and patient experience of lithium, an alternative formulation is needed that better controls release kinetics. Here, we report a novel formulation of lithium that supports longer-term release and does not cause a spike in serum concentration. This formulation integrates lithium ions into a self-assembled metal phenolic network (MPN) (Scheme 1). MPNs are self-assembled nanomaterials formed through the chelation of polyphenols to multivalent metal ions. These materials are tuneable and biocompatible, enabling their use across applications from microbial protection[8,9] to drug delivery.[10] MPNs are especially promising for drug delivery because their disassembly is pH-responsive, enabling targeted release in low-pH environments such as the gut[11,12] or tumor microenvironments.[13] By integrating Li^+ into the MPN matrix for controlled drug delivery, we expand the application of these materials to include ionic drugs. MPN-formulated Li^+ takes advantage of free hydroxy groups in the network, enabling the controlled loading of lithium ions into the matrix. Characterization of our formulation by UV-visible (UV-Vis) spectroscopy, dynamic light scattering (DLS), Fourier-transform infrared (FTIR) spectroscopy, and scanning electron microscopy (SEM) confirm lithium coordination to

[a] Department of Chemical Engineering, Massachusetts Institute of Technology, Cambridge MA, 02139, USA
[b] Center for Environmental Health Sciences, Massachusetts Institute of Technology, Cambridge, MA 02139, USA. E-mail: afurst@mit.edu

† Electronic supplementary information (ESI) available. See DOI: https://doi.org/10.1039/d5tb00901d

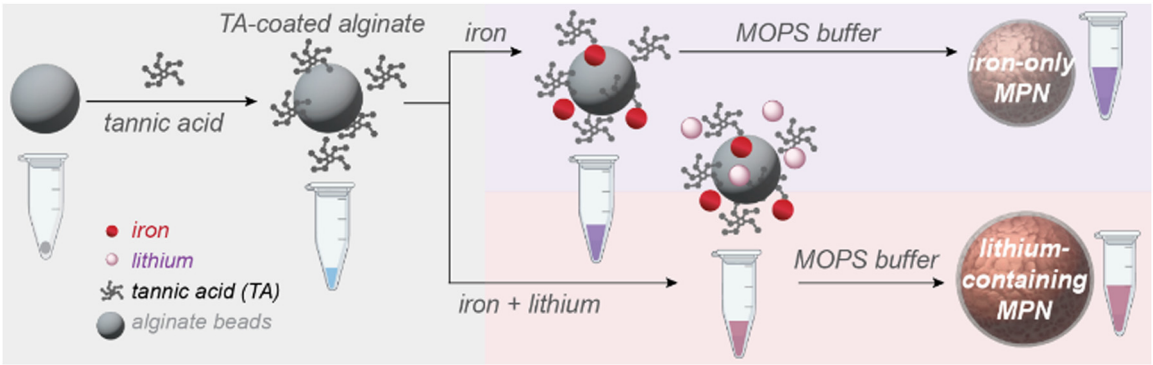

Scheme 1 Preparation of MPN-coated alginate. Alginate beads are initially exposed to tannic acid (TA). To make iron-only MPNs, iron(III) chloride ($FeCl_3$) is then added, followed by MOPS buffer to stabilize the network. To make lithium-containing MPNs, a pre-mixed solution of $FeCl_3$ and LiCl is added to the TA-beads prior to MOPS addition.

deprotonated hydroxyls in the polyphenols. Release studies further demonstrate that this novel formulation results in peak plasma concentrations after 11 hours, nearly twice as long as existing PR formulations, while maintaining serum concentrations within the therapeutic range and avoiding toxic concentration spikes.

Li^+ interactions with phenols have long been studied for applications such as batteries, where transient interactions are desirable.[14–17] In contrast, our material integrates large amounts of Li^+ into an MPN matrix through ionic interactions with alkoxides. Because chelation with multivalent cations is necessary for MPN assembly, it was unclear initially whether MPNs would form as normal in the presence of the ion. Thus, characterizing the generated materials was a critical component of this work. To our knowledge, this study represents the first involving lithium-phenol coordination for therapeutic delivery.

Results and discussion

MPN design

MPNs can be generated with a variety of polyphenols, but the most prevalent and best-studied contain tannic acid (TA), which has a large molecular diameter and 25 phenolic alcohols.[18] This molecule is found in many foods, including coffee and wine, and is generally recognized as safe (GRAS) by the Food and Drug Administration (FDA).[19] Similarly, though a variety of polyvalent metals can be used to form MPNs,[20] Fe^{3+} is one of the most prevalent, mainly due to its low cost, biocompatibility at relevant concentrations, and earth abundance.[21] Further, MPNs comprised of TA and Fe^{3+} are well-characterized, forming 10 nm-thick, two-dimensional assemblies.[22,23] Thus, Fe^{3+}-MPNs (iron-only MPNs) were selected as a biocompatible scaffold for lithium coordination and delivery.

Though iron-only MPNs form reproducible two-dimensional networks, they do not form three-dimensional particles in the absence of a substrate. Thus, for effective delivery, a substrate was needed on which to form the lithium-containing MPNs. Alginate is biocompatible and readily forms microparticles with diverse average diameters and size distributions. We synthesized microparticles with an average diameter of 409 nm to serve as the substrate for MPNs (Scheme 1). When MPNs were formed on the alginate particles with both Li^+ and Fe^{3+} (lithium-containing MPNs), the average particle diameter increased significantly to 4620 nm. We found that Li^+ incorporation was effective if the two cations were incorporated simultaneously.

Particle formation

Because of the significantly increased diameter observed for the lithium-containing particles, we next investigated how the Li^+ integrated into the MPN network. After coating, the MPN-alginate beads were pelleted, and the supernatant was evaluated to determine the extent of Fe^{3+} and TA incorporation into the networks *versus* remaining in the supernatant. The supernatant of the iron-only MPNs was visibly purple, while the lithium-containing formulation yielded colorless supernatant; in contrast, the pellet with lithium-containing formulation was much larger and darker than the pellet for iron-only formulation (Fig. 1a). To confirm MPN formation, UV-Vis measurements were performed. Absorbance spectra show MPNs with and without lithium have an absorbance peak at roughly 300 nm, indicative of the TA phenols, as well as a broad ligand-to-metal charge transfer (LMCT) peak around 550 nm. Consistent with visual observations, a strong absorbance band in the visible region is seen for the supernatant of the iron-only formulation, with little absorbance in this region for the lithium-containing formulation supernatant (Fig. 1b). The absorbance in the visible region of the iron-only MPN supernatant spectrum suggests that not all Fe^{3+} and TA form MPNs on the alginate beads, while the lack of color in the lithium-containing supernatant indicates incorporation of nearly all Fe^{3+} and TA with the alginate. These results are consistent with our observation that lithium-containing pellets have stronger absorbance bands in the visible region (Fig. 1c).

After confirming that addition of Li^+ to MPN formulation promotes incorporation of TA and Fe^{3+}, we optimized our formulation to maximize Li^+ loading. MPN formation was found to be optimal when lithium was added in excess to iron

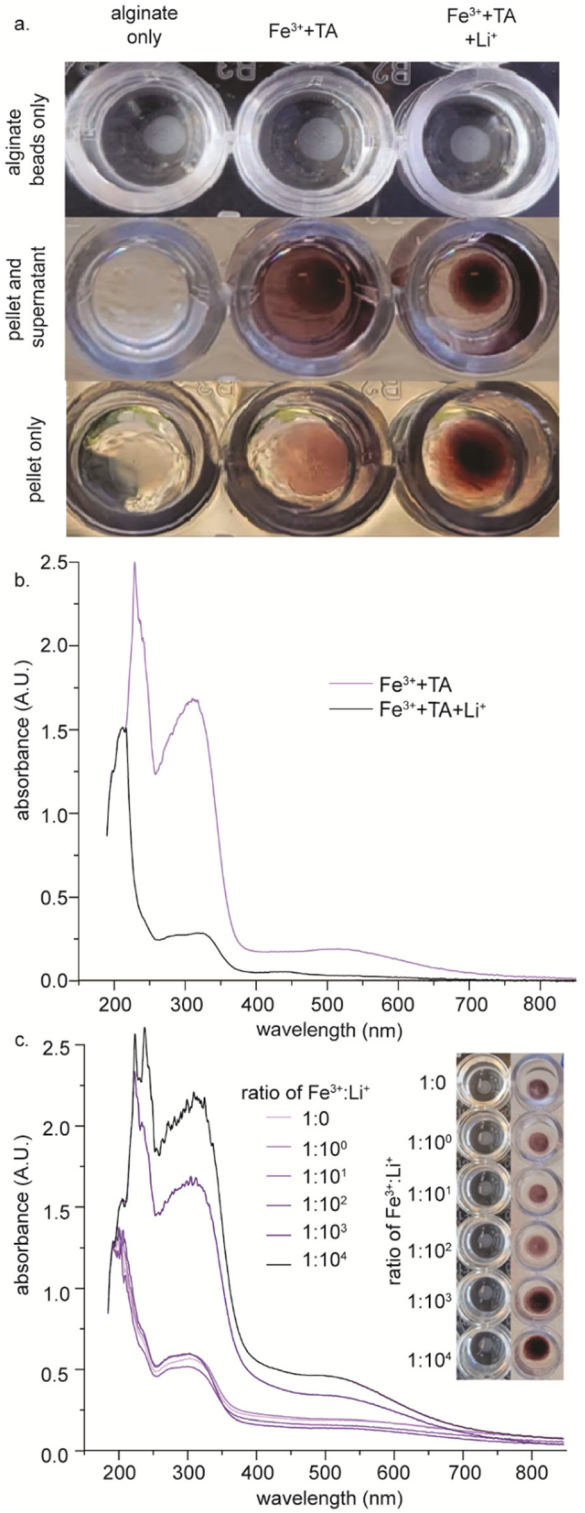

Fig. 1 Formation of lithium-containing MPNs and UV-Vis spectroscopic characterization. (a) Uncoated (left), iron-only (middle), and lithium-containing MPN-coated beads (right) were pelleted in a 96-well plate. Differences in the size, color, and supernatant appearance are apparent between samples. (b) The spectra of the MPN supernatant for the formulations without Li^+ show larger phenol and LMCT absorbance bands than those with Li^+. (c) The amount of lithium added to the formulation is varied. As the concentration of Li^+ increases, so do pellet sizes. UV-Vis spectroscopy shows increasing phenol absorbance and LMCT band of the lithium-containing MPN pellets as the amount of lithium in the formulation is increased.

with a molar ratio starting at 1 : 0 (iron-only formulation) and reaching 1 : 10 000 (lithium-containing formulation). As the amount of lithium is increased from 1 : 10 to 1 : 100, no visible increase in pellet size is observed; however, the pellet size becomes visibly darker and for the 1 : 1000 and 1 : 10 000 formulations compared to the 1 : 0 formulation (Fig. 1c). Consistent with the visual observations, fainter LMCT absorbance bands are observed for the 1 : 0 to 1 : 100 formulations, compared to the 1 : 1000 and 1 : 10 000 formulations (Fig. 1c).

Characterization of lithium incorporation into MPNs

Because larger overall pellet size for the lithium-containing MPNs could be due to larger individual particles or to the presence of networks of particles crosslinked by MPNs, the particles in the pellet were then characterized. Dynamic light scattering (DLS) was used to determine the average particle diameter. The mean diameters for the alginate beads, the iron-only MPNs, and the lithium-containing MPNs were 409 nm, 972 nm, and 4620 nm, respectively (Fig. 2a). A five-fold increase in the diameter upon addition of Li^+ to MPNs indicates differences in the presence of Li^+. We do not generally observe such an increase with MPNs formed from only multivalent ions and polyphenols, indicating a different mode of interaction between lithium and polyphenols.

Based on prior studies of lithium interactions with phenols that show Li^+ coordinating to alkoxides, we hypothesized that the lithium coordinates in the same way here, to phenols not chelated with Fe^{3+} ions.[24] Fourier transform infrared (FTIR) spectroscopy was performed to determine if phenol stretches change in the presence of Li^+. (Fig. 2b).[8] For iron-only MPNs, a broad peak between 3500–3000 cm^{-1} was observed, consistent with hydroxyl stretches. The presence of this band confirms that some unchelated phenols are present in these MPNs. This broad band completely disappears upon incorporation of lithium into the MPNs, with two sharp peaks at 3287 cm^{-1} and 3373 cm^{-1} in the same region. These peaks are consistent with Li^+ interactions with phenolic oxygens, as confirmed from literature of Li^+-ion battery materials that employ TA.[25] Thus, we can conclude that in our lithium-containing MPNs, the Li^+ integrates into the MPN through interactions with the phenolic oxygens.

Two additional differences are observable in the FTIR spectra. The C–C stretching band at 1595 cm^{-1} in the iron-only MPNs disappears, with a more intense split peak in the lithium-containing MPN systems (1622 cm^{-1} and 1650 cm^{-1}). Finally, the C–H stretching band at 1030 cm^{-1} decreases substantially and shifts slightly to 1036 cm^{-1} in the lithium-containing MPN. These changes are consistent with previous work showing transient interactions between deprotonated TA phenols and lithium ions, further supporting our hypothesis that the lithium coordinates to phenols that are not chelated to iron in the MPN matrix.[26] Together, these data, taken in the context of prior studies that show the interaction between Li^+ and polyphenols, indicate that the lithium ions are coordinating to the phenolic groups.[24] Thus, we can conclude that Li^+ integrates into Fe^{3+}-MPNs as hypothesized.

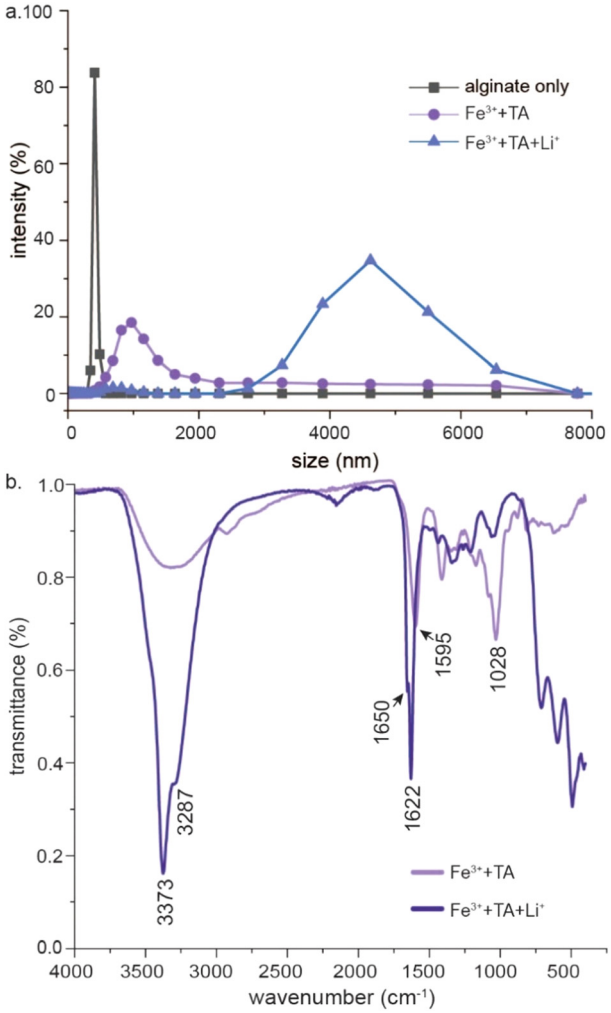

Fig. 2 Coated and uncoated alginate particle characterization. (a) Dynamic light scattering (DLS) measurements show particle size distributions for uncoated alginate beads (gray), iron-only MPN coated beads (light purple), and iron and lithium-MPN coated beads (dark purple). The size distributions for the alginate beads, the iron-only MPN-coated beads, and lithium-containing MPN coated beads had average diameters of 409 nm, 972 nm, and 4620 nm, respectively. (b) Fourier-transform infrared (FTIR) spectra show a difference in MPNs with and without lithium at wavelengths that correspond to OH stretching and C–C stretching when lithium-containing MPN-coated beads (dark purple) are compared to the iron-only MPN coated beads (light purple).

Physical characterization of the MPN particles

Though DLS provides information on the average diameter and size distribution of particles, it does not provide additional detail on their morphology. Thus, to better evaluate the structure of the particles on the micron scale, scanning electron microscopy (SEM) was performed (Fig. 3a). Iron-only MPN samples showed isolated particles with diameters averaging less than 100 μm, which is consistent with the DLS measurements. In contrast, the lithium-containing MPN particles formed large aggregates with diameters approaching the millimeter scale. The surfaces of these aggregates appear amorphous rather than crystalline, leading to additional questions about the distribution of Li^+ throughout the MPN. Thus, energy dispersive X-ray (EDX) analysis was then performed to determine the location of key elements within the imaged particles (Fig. 3b). The iron, oxygen, and chlorine are observable with this technique, but lithium is not due to its small size and similarity to other elements. Calcium was also observable, as it was used as an alginate crosslinking agent. Similar to the SEM images, the morphological differences between the MPNs with and without Li^+ are apparent. In the iron-only MPN formulations, iron, oxygen, and chlorine were distributed evenly across the surface and overlapped with one another, suggesting a uniform MPN coating on the alginate. In contrast, in the lithium-containing MPN samples, iron and oxygen were uniformly distributed across the surface and overlapped with one another, indicating chelated networks of metals and polyphenols. However, the maps of the iron and oxygen showed the inverse of the chlorine elemental map. Thus, for these lithium-containing samples, chlorine was present only where the iron and TA were not. This observation was unexpected, as the elemental distribution was anticipated to be nearly equivalent between the samples. This difference in Cl^- distribution can be explained by its high concentration in lithium-containing samples, as Li^+ was incorporated as the chloride salt. We therefore hypothesize that this high concentration led to the precipitation of chloride crystals.

As EDX can only probe the surface layer of the sample, we sought complementary characterization of the total elemental content in these particles. To quantitatively determine composition, inductively coupled plasma mass-spectroscopy (ICP-MS) was performed, as it measures the composition of the entire sample following dissolution (Fig. 3b). By EDX, the surfaces of the lithium-containing MPN samples had considerably less calcium than the iron-only MPNs, but the ICP-MS-determined total calcium was nearly identical to that of the iron-only MPNs (Fig. 3c). This is consistent with our observation that the lithium-containing MPNs are significantly thicker than the iron-only MPNs, inhibiting observation of elements on the underlying particle. Further, ICP-MS indicates that the lithium is more prevalent on the surface of the MPN-coated beads but does not likely significantly impact their overall elemental distribution, supporting our previous observations that the alginate particles remain intact in these lithium-containing MPN networks.

ICP-MS further validated our previous observations of the pellet size and supernatant content, as the samples containing lithium had considerably more iron than the iron-only MPNs. This finding is consistent with observations that the supernatant for the lithium-containing MPNs did not contain Fe^{3+}–TA. However, these assemblies had only slightly higher levels of iron based on EDX scans (Fig. 3c). This difference between EDX and ICP-MS further indicates that the lithium is not disrupting the interactions between the iron and TA and is only interacting with unchelated phenols. Two hypotheses for the reason that there was such a significant increase in particle diameter in the presence of lithium are as follows. As lithium ions are larger than protons, the increase could be due to the difference in atomic size or particle hydration radius. We also hypothesized that this difference could be due to improved incorporation of

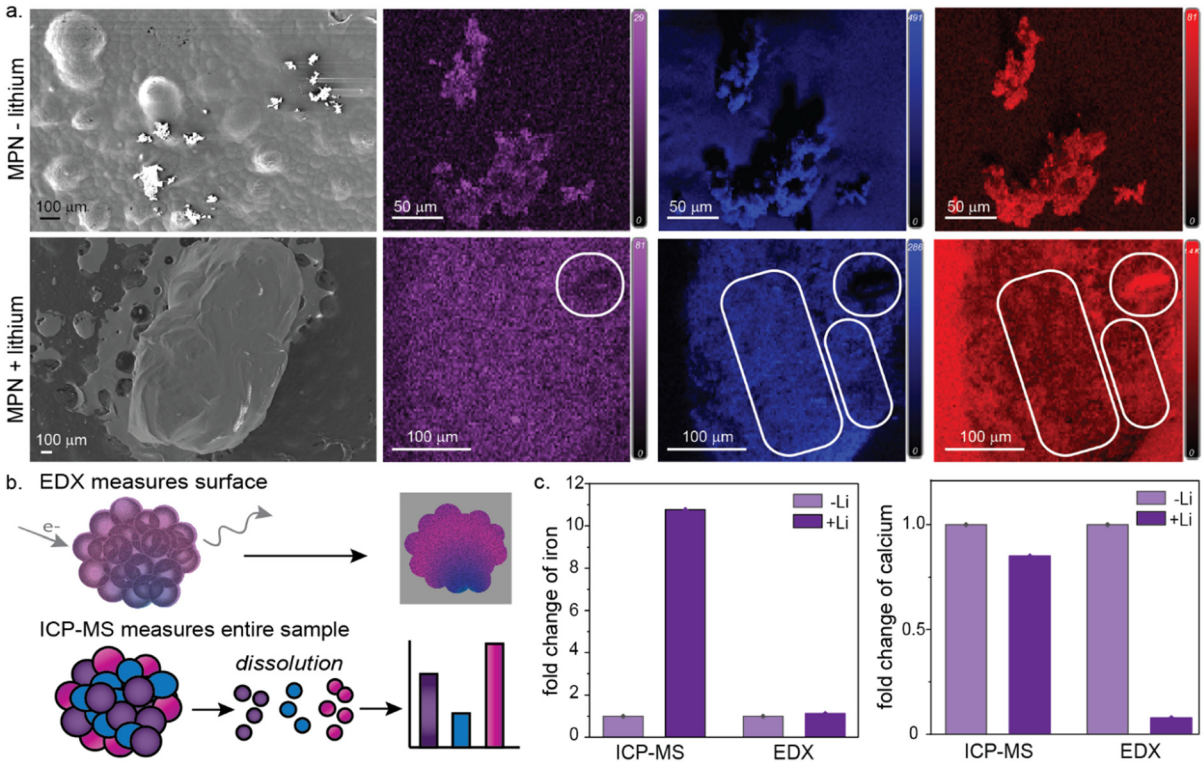

Fig. 3 Physicochemical characterization of MPN-coated beads. (a) SEM and EDX images of iron-only MPNs and lithium-containing MPNs. Iron-only MPNs form particulates on the order of <100 μM, while lithium-containing MPNs form large, amorphous aggregates on the millimeter scale. (b) EDX measures the elemental distribution on the surfaces of the particles, while ICP-MS measures the elemental composition of the entire sample. (c) Elemental quantification of iron and calcium by both EDX and ICP-MS of iron-only MPN beads and lithium-containing MPN beads.

MPN components into the matrix, which is consistent with studies in the literature indicating the formation of thicker iron-TA MPN films in high ionic strength solutions.[22,23] To test these hypotheses, we evaluated differences in the coated alginate beads with and without lithium incorporated. Taken together, physicochemical characterization of these MPN-beads supports our hypothesis that lithium-containing MPNs have similar chemical interactions to the iron-only MPNs but with the addition of lithium ions interacting with unchelated TA phenols. By UV-Vis spectroscopy, lithium supports more efficient incorporation of the Fe^{3+} and TA, with the disappearance of the LMCT band from the supernatant. Further, the large increase in particle diameter for lithium-containing MPNs compared to the iron-only MPNs, as measured by DLS and SEM, confirms morphological differences that were due to the integration of lithium in the particles. Through elemental characterization by EDX and ICP-MS, the surface composition of the iron-only and lithium-containing MPN particles was similar, but overall composition differed in the total amount of iron. With particle morphology and composition fully characterized, we sought to understand the release kinetics of lithium from these materials.

Release kinetics in biological fluids

Despite significant effort to develop PR lithium, current formulations only extend delivery by a few hours and cause a concentration spike in the blood. Because lithium in our lithium-containing MPN particles is formulated in a fundamentally different way (interaction with phenolic oxygens rather than with an inorganic ion as a salt), the release kinetics were anticipated to differ significantly from existing formulations. An additional consideration for MPN-based delivery is the acid lability of these materials. Thus, in addition to evaluating the lithium release from the MPN, we investigated commercially available, delayed-release capsules to protect the MPNs from rapid degradation in the acidic conditions of the stomach (Fig. 4a), which could result in undesirable burst release into the bloodstream.

For the MPN formulation, we hypothesized that we could tune our formulation to allow for selective, controlled release in the upper intestinal track and serum *via* incorporation of a hydrogel that encases the MPN-alginate particles to control release in both upper intestinal fluid and serum. *In vitro* studies were performed to evaluate these hypotheses. For both hydrogel-encased and unencased lithium-containing MPN particles, simulated upper intestinal fluid and serum were used for release profiles.

Lithium release kinetics were then evaluated by performing ICP-MS on simulated intestinal fluid as well as serum for both hydrogel-encased lithium-containing MPN particles and lithium-containing MPN particles without external hydrogels. As expected, incorporation of the lithium-containing MPNs into the hydrogels

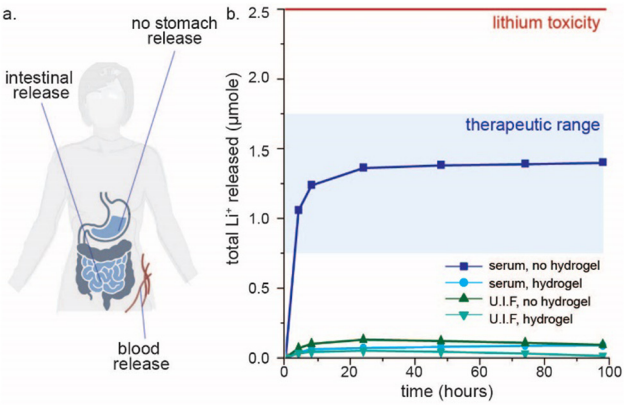

Fig. 4 Drug release kinetics in simulated bodily fluids. (a) Our formulation consists of tuneable components that allow for selectively controlled release in the stomach, the upper intestine, and serum. (b) Encasing the lithium-containing particles in a hydrogel slows their release in simulated upper intestinal fluid (U. I. F). Our formulation showed controlled release in the intestinal fluid and reached peak serum lithium concentrations in over 20 hours and maintained serum lithium levels in the therapeutic window over several days.

slowed release in both intestinal fluid and serum (Fig. 4b), indicating a tunable parameter for controlled release of lithium. Importantly, lithium release in the intestinal fluid was well below the therapeutic range, even for lithium-containing MPN particles without hydrogel encapsulation (Fig. 4b), indicating favorable and controlled release that would prevent a dangerous spike in serum lithium concentrations. The amount of lithium released in the upper intestinal fluid was low enough to be near the detection limit of the ICP-MS (Fig S2, ESI†).

Conclusions

Despite the global impact of BD, there has been minimal effort devoted to improving lithium formulation to decrease toxicity risk and improve the patient experience. Here, we report a novel formulation for controlled lithium delivery through integration of lithium ions into an MPN matrix. Characterization of these materials confirms that the lithium is stably incorporated into the network through interaction with phenolic oxygens. Complete physicochemical characterization enabled the precise determination of lithium loading into these networks and the consistency of their assembly. Further, we find the hydrogel-based formulation enables stable delivery in both intestinal fluid and serum. Our formulation does not exhibit burst release into the intestinal fluid, but rather slow and steady release in the serum within the therapeutic range. Using unencapsulated lithium-containing MPN particles, peak serum lithium concentrations are achieved gradually over 20 hours while maintaining therapeutically relevant concentrations and circumventing potentially toxic concentration spikes. These serum levels are maintained for over four days, ten times longer than current prolonged release lithium. These improvements decrease the risk of toxicity to patients and control the serum concentration over long time periods to improve patient experience. This work represents the first major breakthrough in lithium formulation in decades, and the multi-faceted nature of our formulation allows unprecedented control over lithium release.

Author contributions

The manuscript was written through contributions of all authors.

Conflicts of interest

There are no conflicts of interest to declare.

Data availability

Data that support the findings of this study are available from the corresponding author upon reasonable request.

Acknowledgements

This work was supported by the National Institutes of Health New Innovator Award (1DP2GM154015-01), an NIEHS Core Center Grant (P42-ES027707) and the NIH-NIEHS Superfund Research Program Grant (P42-ES027707). M. Z. was supported by an NIEHS Training Grant, Grant # T32 ES007020.

References

1 Bipolar disorder: MedlinePlus Genetics. https://medlineplus.gov/genetics/condition/bipolar-disorder/(accessed 2024-01-09).
2 Bipolar Disorder Statistics. Depression and Bipolar Support Alliance. https://www.dbsalliance.org/education/bipolar-disorder/bipolar-disorder-statistics/(accessed 2023-08-15).
3 L. Bessonova, K. Ogden, M. J. Doane, A. K. O'Sullivan and M. Tohen, The Economic Burden of Bipolar Disorder in the United States: A Systematic Literature Review. Clin. Outcomes Res, *CEOR*, 2020, **12**, 481–497, DOI: 10.2147/CEOR.S259338.
4 W. A. Nolen, More Robust Evidence for the Efficacy of Lithium in the Long-Term Treatment of Bipolar Disorder: Should Lithium (Again) Be Recommended as the Single Preferred First-Line Treatment, *Int. J. Bipolar Disord.*, 2015, **3**, 1, DOI: 10.1186/s40345-014-0017-6.
5 S. A. Hedya; A. Avula and H. D. Swoboda, *Lithium Toxicity StatPearls*, StatPearls Publishing, Treasure Island, 2023.
6 K. Chokhawala; S. Lee and A. Saadabadi, *Lithium. In StatPearls*, StatPearls Publishing, Treasure Island (FL), 2023.
7 P. Girardi, R. Brugnoli, G. Manfredi and G. Sani, Lithium in Bipolar Disorder: Optimizing Therapy Using Prolonged-Release Formulations, *Drugs RD*, 2016, **16**(4), 293–302, DOI: 10.1007/s40268-016-0139-7.
8 G. Fan, P. Wasuwanich, M. R. Rodriguez-Otero and A. L. Furst, Protection of anaerobic microbes from processing

stressors using metal–phenolic networks, *J. Am. Chem. Soc.*, 2022, **144**(6), 2438–2443, DOI: **10.1021/jacs.1c09018**.

9 B. Burke, G. Fan, P. Wasuwanich, E. B. Moore and A. L. Furst, Self-assembled nanocoatings protect microbial fertilizers for climate-resilient agriculture, *JACS Au*, 2023, **3**(11), 2973–2980, DOI: **10.1021/jacsau.3c00426**.

10 P. Liu, X. Shi, S. Zhong, Y. Peng, Y. Qi, J. Ding and W. Zhou, Metal-Phenolic Networks for Cancer Theranostics, *Biomater. Sci.*, 2021, **9**(8), 2825–2849, DOI: **10.1039/D0BM02064H**.

11 A. Ali, R. Javed, S. Farhangi, T. Shah, S. Ullah, N. Ul Ain, T. Liu, Z. Guo, I. Lynch, F. Raza, P. Zhang and Y. Rui, Metal Phenolic Networks (MPNs)-Based pH-Sensitive Stimulus Responsive Nanosystems for Drug Delivery in Tumor Microenvironment, *J. Drug Deliv. Sci. Technol.*, 2023, **84**, 104536, DOI: **10.1016/j.jddst.2023.104536**.

12 Y. Chang, P. Cui, S. Zhou, L. Qiu, P. Jiang, S. Chen, C. Wang and J. Wang, Metal-Phenolic Network for Cancer Therapy, *J. Drug Deliv. Sci. Technol.*, 2023, **81**, 104194, DOI: **10.1016/j.jddst.2023.104194**.

13 L. Shen, Y. Zhang, J. Feng, W. Xu, Y. Chen, K. Li, X. Yang, Y. Zhao, S. Ge and J. Li, Microencapsulation of Ionic Liquid by Interfacial Self-Assembly of Metal-Phenolic Network for Efficient Gastric Absorption of Oral Drug Delivery, *ACS Appl. Mater. Interfaces*, 2022, **14**(40), 45229–45239, DOI: **10.1021/acsami.2c15599**.

14 N. Kana, S. Olivier-Archambaud, T. Devic and B. Lestriez, Tannic Acid as a Binder and Electronic Conductor Precursor in Silicon Electrodes for Li-Ion Batteries, *Electrochem. Commun.*, 2023, **151**, 107495, DOI: **10.1016/j.elecom.2023.107495**.

15 K. T. Sarang, X. Li, A. Miranda, T. Terlier, E.-S. Oh, R. Verduzco and J. L. Lutkenhaus, Tannic Acid as a Small-Molecule Binder for Silicon Anodes, *ACS Appl. Energy Mater.*, 2020, **3**(7), 6985–6994, DOI: **10.1021/acsaem.0c01051**.

16 E. Prasetyo, W. A. Muryanta, A. G. Anggraini, S. Sudibyo, M. Amin and M. Al Muttaqii, Tannic Acid as a Novel and Green Leaching Reagent for Cobalt and Lithium Recycling from Spent Lithium-Ion Batteries, *J. Mater. Cycles Waste Manag.*, 2022, **24**(3), 927–938, DOI: **10.1007/s10163-022-01368-y**.

17 Z. Xu, H. Ye, H. Li, Y. Xu, C. Wang, J. Yin and H. Zhu, Enhanced Lithium Ion Storage Performance of Tannic Acid in LiTFSI Electrolyte, *ACS Omega*, 2017, **2**(4), 1273–1278, DOI: **10.1021/acsomega.6b00504**.

18 P. Wasuwanich, G. Fan, B. Burke and A. L. Furst, Metal-Phenolic Networks as Tuneable Spore Coat Mimetics, *J. Mater. Chem. B*, 2022, **10**(37), 7600–7606, DOI: **10.1039/D2TB00717G**.

19 Z. Guo, W. Xie, J. Lu, X. Guo, J. Xu, W. Xu, Y. Chi, N. Takuya, H. Wu and L. Zhao, Tannic Acid-Based Metal Phenolic Networks for Bio-Applications: A Review, *J. Mater. Chem. B*, 2021, **9**(20), 4098–4110, DOI: **10.1039/D1TB00383F**.

20 J. Qin, N. Guo, J. Yang and Y. Chen, Recent Advances of Metal–Polyphenol Coordination Polymers for Biomedical Applications, *Biosensors*, 2023, **13**(8), 776, DOI: **10.3390/bios13080776**.

21 W. Chen, M. Liu, H. Yang, A. Nezamzadeh-Ejhieh, C. Lu, Y. Pan, J. Liu and Z. Bai, Recent Advances of Fe(III)/Fe(II)-MPNs in Biomedical Applications, *Pharmaceutics*, 2023, **15**(5), 1323, DOI: **10.3390/pharmaceutics15051323**.

22 T. Park, W. I. Kim, B. J. Kim, H. Lee, I. S. Choi, J. H. Park and W. K. Cho, Salt-Induced, Continuous Deposition of Supramolecular Iron(III)-Tannic Acid Complex, *Langmuir ACS J. Surf. Colloids*, 2018, **34**(41), 12318–12323, DOI: **10.1021/acs.Langmuir.8b02686**.

23 J. Guo, J. J. Richardson, Q. A. Besford, A. J. Christofferson, Y. Dai, C. W. Ong, B. L. Tardy, K. Liang, G. H. Choi, J. Cui, P. J. Yoo, I. Yarovsky and F. Caruso, Influence of Ionic Strength on the Deposition of Metal–Phenolic Networks, *Langmuir*, 2017, **33**(40), 10616–10622, DOI: **10.1021/acs.Langmuir.7b02692**.

24 I. K. Ilic, A. Tsouka, M. Perovic, J. Hwang, T. Heil, F. F. Loeffler, M. Oschatz, M. Antonietti and C. Liedel, Sustainable Cathodes for Lithium-Ion Energy Storage Devices Based on Tannic Acid—Toward Ecofriendly Energy Storage, *Adv. Sustainable Syst.*, 2021, **5**(1), 2000206, DOI: **10.1002/adsu.202000206**.

25 Y. Wang, C. Cui, R. Cheng, J. Wang and X. Wang, Tannic Acid-Derived Carbon Coating on LiFePO4 Nanocrystals Enables High-Rate Cathode Materials for Lithium-Ion Batteries, *ACS Appl. Nano Mater.*, 2023, **6**(11), 9124–9129, DOI: **10.1021/acsanm.3c01372**.

26 F. Weber, E. Sagstuen, Q.-Z. Zhong, T. Zheng and H. Tiainen, Tannic Acid Radicals in the Presence of Alkali Metal Salts and Their Impact on the Formation of Silicate-Phenolic Networks, *ACS Appl. Mater. Interfaces*, 2020, **12**(47), 52457–52466, DOI: **10.1021/acsami.0c16946**.

